Ocean Engineering 211 (2020) 107627

Contents lists available at ScienceDirect

Ocean Engineering

journal homepage: www.elsevier.com/locate/oceaneng

Event-triggered composite adaptive fuzzy control of sailboat with heeling constraint

Yingjie Deng [a], Xianku Zhang [a,*], Qiang Zhang [b], Yancai Hu [b]

[a] Navigation College, Dalian Maritime University, Dalian, 116026, Liaoning, China
[b] Navigation College, Shandong Jiaotong University, Weihai, 264209, Shandong, China

ARTICLE INFO

Keywords:
Sailboat
Event-triggered control (ETC)
Composite adaptive fuzzy control
Heeling constraint
Input saturation

ABSTRACT

In this paper, the event-triggered composite adaptive fuzzy control laws are developed to control both the surge speed and the heading angle of the sailboat. The fuzzy logic systems (FLSs) are employed to approximate the nonlinearities in the model of the sailboat. To enhance the approximating accuracy, a serial–parallel estimation model is established at first, and the composite adaptive laws of the FLS weights are then derived by combining the tracking errors with the prediction errors between the estimation model and the dynamic loop of the sailboat. To prevent the sailboat from capsizing, we consider the heeling constraint in the roll motion during the voyage. By using the backstepping method, the heeling constraint is transformed to the input saturation of the sail. The auxiliary systems are fabricated to offset the input saturation of the sail and the rudder, which are incorporated into the control laws. To reduce the acting frequencies of the actuators, the control laws for the sail and the rudder are designed in the event-triggered form, and the triggering conditions are constructed separately. The uncertain gain of the rudder is estimated by the adaptive laws. The proposed control scheme can guarantee the semi-global uniformly ultimate boundedness (SGUUB) of all the errors. Through the numerical path-following test, the effectiveness of the proposed scheme is verified.

1. Introduction

The navigational cybernetics have been rapidly developing since the human society entered the third industrial revolution. Nowadays, the ship tends to be more versatile and intelligent than its past. Throughout the development of navigational cybernetics, much experience was drawn from the advanced control techniques for generic nonlinear systems, such as Jiang (2002), Do (2010) and Deng et al. (2019a) and the references therein. In the background of energy crisis, the saving of energy becomes one of the keynote development themes of navigational cybernetics. For this theme, the wind-assisted ship is more competitive than the common-powered ship, especially in the long-term and wide-range task. However, in contrast to numerous researches on the control of the common-powered ship, it lacks experience to control the sailboat, which is pretty challenging due to the variability and uncontrollability of the wind.

Following the separate principle, the control of the sailboat can be divided into two aspects of the sail and the rudder. Regardless of coupling, the surge motion of the sailboat is mainly controlled by the sail and the yaw motion by the rudder. For the sail, the control input boils down to the sheeting angle of the sail. The existing researches mostly concentrated on maximizing the surge speed of the sailboat, and some optimization algorithms of the sheeting angle were proposed, such as the quantified set inversion in Herrero et al. (2010), the extremum seeking in Xiao et al. (2012), Corno et al. (2016), Deng et al. (2019c) and Shen et al. (2019). Nevertheless, the surge speed cannot be controlled to a specific value in these researches. As the strong maneuverability is required for a sailboat in the busy water (Zhang et al., 2018), this control objective is pretty realistic and can be achieved based on the known aerodynamics of the sail. In Deng et al. (2019e), an event-triggered robust fuzzy control scheme was proposed to control the surge speed of the wing-sailed catamaran, where the FLS was employed to approximate the nonlinearity in the surge motion. Because the roll motion was exempted for the wing-sailed catamaran, this approach cannot extend to the mono-hull sailboat. The roll motion of the mono-hull sailboat is strongly influenced by the regulation of the sail, for which the constraint of the heeling angle should be considered. Thus, the previous optimization and control algorithms are not practical for the sailboat, and may result in capsizing sometimes. As we have learnt, Stelzer et al. (2007) used the FLS to describe the tuning principle for the sail, which chose the heeling angle as the input. Although the heeling constraint was addressed in this scheme, it was

* Corresponding author.
E-mail addresses: dyj_dl@126.com (Y. Deng), zhangxk@dlmu.edu.cn (X. Zhang).

https://doi.org/10.1016/j.oceaneng.2020.107627
Received 13 October 2019; Received in revised form 6 June 2020; Accepted 8 June 2020
Available online 11 June 2020

based on artificial expertise and may degrade the propulsion efficiency of the sail.

For the rudder, the control input boils down to the rudder angle. Without the model of the sailboat, Elkaim and Kelbley (2006), Cruz and Alves (2010) and Jaulin and Bars (2013) designed the PID controller for the rudder, Stelzer et al. (2007) designed the FLS-based rudder controller. With the deterministic model, Herrero et al. (2010) referred to the feedback linearization method to design the controller, Xiao and Jouffroy (2011) and He et al. (2012) designed the backstepping-based controllers for the rudder and the weight balancing system respectively. To deal with the uncertainties, Xiao and Jouffroy (2014) developed a robust control scheme by tuning the parameters, and Deng et al. (2019e) resorted to the robust fuzzy damping technique. Nevertheless, these schemes were conservative and may result in the unnecessarily large control inputs. In Deng et al. (2019d), the adaptive neural rudder controller was designed with the minimum learning parameters, where the control performance was strongly concerned with the approximating accuracy of the neural networks (NNs). However, the adaptive law therein can only guarantee the closed-loop stability, rather than the identification of the model uncertainties and the interpretability of the NNs. This problem has been discussed for the strict-feedback nonlinear systems in Xu et al. (2014), Li and Tong (2015) and Li et al. (2016), where the composite learning was proposed as a solution. Because the model of the sailboat does not belong to the strict-feedback system, these approaches cannot be directly applied to the control of the sailboat. To our knowledge, there is no such attempt at present. Another problem of the above researches consists in the uncertainty of the rudder. In Xiao and Jouffroy (2014), the nonlinearity of the rudder was simplified as a sine function. Deng et al. (2019d) assumed that the fitting error between the sine function and the lift coefficient of the rudder was upper-bounded by a known constant. Deng et al. (2019e) assumed that both the upper and lower bounds of the gain of the rudder were known. These schemes utilized the robust design to offset the uncertainty of the rudder.

In compliance with the nautical practice, the input saturation should be considered in the above control schemes. Although He et al. (2012), Jaulin and Bars (2013), Xiao and Jouffroy (2014), Saoud et al. (2015) and Deng et al. (2019c,d) constrained the operating range of the rudder, these schemes did not analyze the influence of the input saturation on the stability. In Ma et al. (2019) and Deng et al. (2019a,e), the sigmoid functions were introduced to approximate the saturation nonlinearities of the actuators. Through the mean value theorem, the saturation nonlinearity was transformed to the formula with the bounded gain and the approximating error. In Zheng et al. (2018), the uncertainty observer was fabricated to offset the lumped uncertainties including the control error through the input saturation. Yan and Wang (2012) and Peng et al. (2019) studied the model predictive control for surface and underwater marine crafts, where the tracking control was transformed to the neurodynamic optimization with a series of constraints including the input saturation. Nevertheless, the above methods cannot be applied to the adaptive control of the sailboat. Another practical issue consists in the acting frequency of the actuator. The lower acting frequency will reduce the mechanical wear and elongate the service life of the actuator. The event-triggered control provides a solution to this problem. This method functions in an intelligent manner, where the control happens only when the triggering condition is violated, and it was introduced to the navigational cybernetics in Jiao and Wang (2016a,b), Deng et al. (2019a) and Guo et al. (2019). Due to the variability of the wind, the acting of the actuators in the sailboat is more frequent than that in the common-powered ship. Thus, the ETC is more significant for the sailboat. Deng et al. (2019e) first investigated the ETC for the wing-sailed catamaran, and combined the ETC with the robust fuzzy damping. Although Li and Yang (2018) and Cao et al. (2018) have combined the ETC with the adaptive NNs or FLSs for the pure-feedback and strict-feedback systems, this issue is left to be considered for the sailboat.

Motivated by the above challenges, this paper develops a unified event-triggered adaptive fuzzy control scheme for the sailboat. A serial–parallel estimation model is established for the dynamic loop of the sailboat. On this basis, we derive the composite adaptive laws of the FLS weights. In this paper, the heeling constraint is transformed to the input saturation of the sail. The auxiliary systems are constructed to offset the control error through the input saturation. The adaptive laws are fabricated to estimate the uncertain gain of the rudder. The contribution of this paper is mainly threefold. (1) Compared with the existing adaptive neural and fuzzy control schemes for marine crafts, the composite learning of the FLSs can ensure both the closed-loop stability and the identification of the uncertainties, such that the tracking performance is improved. Compared with Deng et al. (2019e), the adaptive design circumvents the conservatism of the robust design. (2) Compared with the existing control schemes for the sailboat, this scheme addresses the heeling constraint of the sailboat and strictly proves the boundedness of its heeling angle, which can prevent the sailboat from capsizing and is more secure. (3) This scheme synthesizes several practical issues, including the input saturation, the acting frequency of the actuator and the uncertain gain of the rudder. Thus, it is more versatile and credible than the existing control schemes for the sailboat.

Notations: Uniformly in this paper, $\mathrm{sign}(s)$ denotes the sign function of the element of s, $\|s\|$ denotes the 2 norm, $\inf\{s\}$ denotes the infimum, and $\hat{s}$ denotes the estimation of s, where $\tilde{s} = s - \hat{s}$ implies the estimating error.

2. Preliminaries

2.1. Mathematical model of sailboat

According to Deng et al. (2019d), the mathematical model of a sailboat can be described in two frames with 4 degrees of freedom. The position and attitudes of the sailboat can be described in the earth frame, seeing the differential equations in Eq. (1), which is also called the kinematic loop. The kinematic states of the sailboat can be described in the body frame, seeing Eq. (2), which is also called the dynamic loop.

$$\begin{cases} \dot{x} = u\cos(\psi) - v\cos(\phi)\sin(\psi) \\ \dot{y} = u\sin(\psi) + v\cos(\phi)\cos(\psi) \\ \dot{\phi} = p \\ \dot{\psi} = r\cos(\phi) \end{cases} \tag{1}$$

$$\begin{cases} m_u\dot{u} = F_{xs} + F_{xr} + m_v vr + F_{xh} + F_{wu} \\ m_v\dot{v} = F_{ys} + F_{yr} - m_u ur + F_{yh} + F_{wv} \\ m_p\dot{p} = M_{xs} + M_{xr} - a|p|p - b\phi^2 - c\phi + M_{xh} + M_{wp} \\ m_r\dot{r} = M_{zr} + M_{zs} + (m_u - m_v)uv - d|r|r\cos(\phi) \\ \qquad + M_{zh} + M_{wr} \end{cases} \tag{2}$$

where all the variables are defined in Table 1 and illustrated in Fig. 1. In Eq. (2), m_i with $i = u, v, p, r$ can be calculated by empirical equations and the other parameters are deemed to be unknown. Denote the simplified disturbances as $d_{wu} = F_{wu}/m_u$, $d_{wv} = F_{wv}/m_v$, $d_{wp} = M_{wp}/m_p$ and $d_{wr} = M_{wr}/m_r$, and they are assumed to be bounded with $|d_{wi}| < \bar{d}_{wi}$, where $\bar{d}_{wi}$ is a positive constant.

Following the separate principle, we can deem that F_{xs} dominates the surge motion in Eq. (2), M_{xs} the roll motion and M_{zr} the yaw motion. It should be noted that the sway motion satisfies the passive boundedness (Li et al., 2008), that means v is self-constrained while the other motions are bounded. The relationship between F_{xs} and M_{xs} are shown in Eq. (3).

$$\begin{cases} F_{xs} = L_s\sin(\alpha_{aw}) - D_s\cos(\alpha_{aw}) \\ M_{xs} = -z_s(L_s\cos(\alpha_{aw}) + D_s\sin(\alpha_{aw})) \end{cases} \tag{3}$$

Table 1
Definitions of variables.

Notations	Descriptions
(x, y)	Coordinates of X and Y axes in the earth frame
ψ, ϕ	Heading and heeling angles
z_s	z Coordinate of COE in the body frame
u, v, p, r	Surge and sway speeds, roll and yaw rates
m_i	Inertia of sailboat including additional mass and moment, $i = u, v, p, r$
a, b, c, d	Constants of restoring effect
F_{xj}, F_{yj}	Forces along surge and sway imposed on rudder, sail and hull, $j = r, s, h$
M_{xj}, M_{zj}	Moments of roll and yaw on components
F_{wi}, M_{wi}	Disturbing forces and moments, $i = u, v, p, r$
U_{aw}	Apparent wind speed
α_{aw}	Bearing angle of apparent wind to sailboat
α_s	Attacking angle of apparent wind to sail
δ_s, δ_r	Sheeting angle of sail and rudder angle
L_s, D_s	Lift and drag imposed on sail
CG	Center of gravity
COE	Center of effect on wing-sail

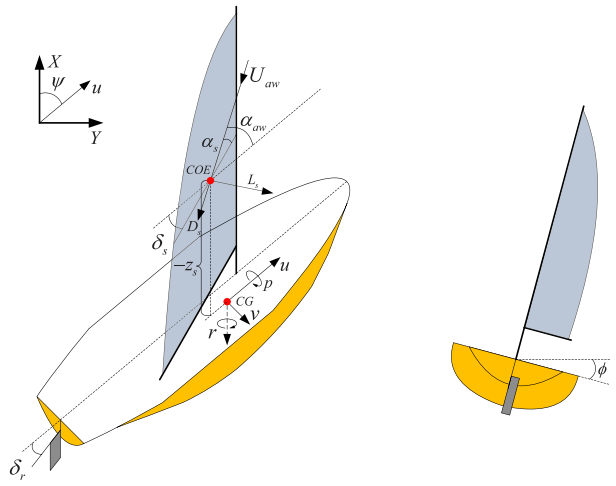

Fig. 1. Illustration of variables.

where L_s and D_s are further expressed as

$$\begin{cases} L_s = \frac{1}{2}\rho_a A_s U_{aw}^2 C_{Ls} \\ D_s = \frac{1}{2}\rho_a A_s U_{aw}^2 C_{Ds} \end{cases} \tag{4}$$

where A_s is the unilateral surface area of the sail. Because the speed of the sailboat is relatively slow, the lift and the drag coefficients of C_{Ls} and C_{Ds} are irrelevant to U_{aw} and depicted as the functions of α_s (Stevens et al., 2016). Through the aerodynamic calculation or the wind tunnel test, the numerical relationship between these coefficients and α_s can be known. Thus, both F_{xs} and M_{xs} can be obtained through calculation. From Fig. 1, it has $\delta_s = \alpha_{aw} - \alpha_s$. For any δ_s in the selecting range of Ω_s, one can always find its one-to-one mapping to F_{xs}. The selecting range of Ω_s will be discussed in the next section. Because U_{aw} is finite in Eq. (4), the input of F_{xs} satisfies the saturation constraint of Eq. (5).

$$\hat{F}_{xs} = \begin{cases} \bar{F}_{xs}, & F_{xs}^c \geq \bar{F}_{xs} \\ F_{xs}^c, & 0 < F_{xs}^c < \bar{F}_{xs} \\ 0, & F_{xs}^c \leq 0 \end{cases} \tag{5}$$

where F_{xs}^c is the desired value of F_{xs}. Denote the value of F_{xs}^c through the saturation as $\hat{F}_{xs}$. The relationship between F_{xs} and $\hat{F}_{xs}$ will be discussed later in the ETC design. $\bar{F}_{xs} > 0$ is the upper bound of $\hat{F}_{xs}$ at the current time, which relates to the constraint of M_{xs} and is designed later. If the sail starts luffing and flapping downwind, namely $\alpha_s = 0$, both F_{xs} and M_{xs} equate to 0. Thus, the lower bound of $\hat{F}_{xs}$ is set to be 0.

For the turning torque of M_{zr}, it can be expressed as $M_{zr} = c_r \delta_{r2}$, where $\delta_{r2} = |\delta_r|\delta_r$ and c_r is the unknown gain. The input of δ_{r2} satisfies the saturation constraint of Eq. (6).

$$\hat{\delta}_{r2} = \begin{cases} \bar{\delta}_{r2}, & \delta_{r2}^c \geq \bar{\delta}_{r2} \\ \delta_{r2}^c, & -\bar{\delta}_{r2} < \delta_{r2}^c < \bar{\delta}_{r2} \\ -\bar{\delta}_{r2}, & \delta_{r2}^c \leq -\bar{\delta}_{r2} \end{cases} \tag{6}$$

where δ_{r2}^c is the desired value of δ_{r2}, and $\bar{\delta}_{r2} > 0$ is the upper bound of $\hat{\delta}_{r2}$. Then, the control objective of this paper can be concluded as follows.

Control Objective: For the desired surge speed u_d and the desired heading angle ψ_d of the sailboat, the ETC laws of δ_s and δ_{r2} can ensure the convergence of u and ψ to u_d and ψ_d, namely the tracking errors of $u_e = u - u_d$ and $\psi_e = \psi - \psi_d$ are ultimately bounded. Besides, the heeling angle ϕ of the sailboat should be constrained in a preset range without the risk of capsizing during the voyage.

2.2. FLS approximation

According to Li and Tong (2015) and Deng et al. (2019e), the FLS is comprised of four parts, i.e. the base of fuzzy rules, the fuzzier, the fuzzy reasoning machine and the defuzzier. For a multiple-inputs-single-output system, the FLS can be transformed to Eq. (7).

$$y_f(\boldsymbol{x}) = \frac{\sum_{i=1}^N w_i s_i(\boldsymbol{x})}{\sum_{i=1}^N s_i(\boldsymbol{x})} \tag{7}$$

where y_f is the output, $\boldsymbol{x}$ is the input vector, N is the number of fuzzy rules, w_i is the weight of the ith fuzzy rule and $s_i(\boldsymbol{x})$ denotes the product of all the membership functions in the ith fuzzy rule. Define $\varphi_i = s_i(\boldsymbol{x}) / \sum_{i=1}^N s_i(\boldsymbol{x})$, $\boldsymbol{\varphi} = [\varphi_1, \ldots, \varphi_N]^{\mathrm{T}}$ and $\boldsymbol{W} = [w_1, \ldots, w_N]^{\mathrm{T}}$. Eq. (7) can be simplified as $y_f = \boldsymbol{W}^{\mathrm{T}}\boldsymbol{\varphi}$. Then, the universal approximation theorem of the FLS can be described as the following lemma.

Lemma 1 (*Wang, 1994*). *For any continuous function of $f(\boldsymbol{x})$ defined in a compact set, there always exists a FLS satisfying*

$$f(\boldsymbol{x}) = \boldsymbol{W}^{\mathrm{T}}\boldsymbol{\varphi} + \varepsilon$$

where ε is the approximating error and can be bounded by an arbitrarily small positive constant, namely $|\varepsilon| \leq \bar{\varepsilon}$.

3. Control design

3.1. Heeling constraint

To prevent the sailboat from capsizing, the heeling constraint of ϕ is addressed in this part. A preset threshold of ϕ was denoted by $\bar{\phi}$, where $0 < \bar{\phi} < \pi/2$. This threshold should be determined by assessing the capsizing risk. Our goal is to keep the varying range of ϕ to approach the ideal range of $[-\bar{\phi}, \bar{\phi}]$ as close as possible.

It can be inferred from Eq. (1) that ϕ is determined by the roll rate of p. Through the backstepping method, we can design the thresholds of p as

$$\begin{cases} \bar{p} = k_p(\bar{\phi} - \phi) \\ \underline{p} = -k_p(\bar{\phi} + \phi) \end{cases} \tag{8}$$

where $k_p > 0$ is the tuning parameter. In Eq. (8), $\bar{p} > \underline{p}$ always exists. By differentiating $\bar{p}$ and $\underline{p}$, it renders $\dot{\bar{p}} = \dot{\underline{p}} = -k_p p$. It is clear that $\phi \in [-\bar{\phi}, \bar{\phi}]$ while $p \in [\underline{p}, \bar{p}]$. From Eq. (2), we know that p is mainly dominated by M_{xs}. According to Lemma 1, the nonlinearity of the roll motion in Eq. (2) can be expressed as the FLS of Eq. (9).

$$\boldsymbol{W}_p^{\mathrm{T}}\boldsymbol{\varphi}_p(\upsilon) + \varepsilon_p = \frac{M_{xr} - a|p|p - b\phi^2 - c\phi + M_{xh}}{m_p} \tag{9}$$

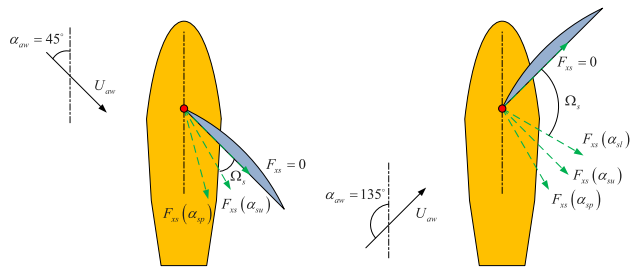

(a) upwind case (b) downwind case

Fig. 2. Selecting range of sail sheeting angle.

where $\upsilon = [\phi, u, v, p, r, U_{aw}, \alpha_{aw}]^{\mathrm{T}}$. Ideally to make $p \in [\underline{p}, \bar{p}]$, the thresholds of M_{xs} are designed as

$$\begin{cases} \bar{M}_{xs} = m_p(k_{\dot{p}}\bar{p} - (k_{\dot{p}} + k_p)p - \hat{\boldsymbol{W}}_P^{\mathrm{T}}\boldsymbol{\varphi}_p) \\ \underline{M}_{xs} = m_p(k_{\dot{p}}\underline{p} - (k_{\dot{p}} + k_p)p - \hat{\boldsymbol{W}}_P^{\mathrm{T}}\boldsymbol{\varphi}_p) \end{cases} \tag{10}$$

where $k_{\dot{p}} > 0$ is the tuning parameter. In Eq. (10), $\bar{M}_{xs} > \underline{M}_{xs}$ always holds. The constrained varying range of M_{xs} is determined as $M_{xs} \in [\underline{M}_{xs}, \bar{M}_{xs}]$.

While M_{xs} is constrained, $\bar{F}_{xs}$ can be determined. Regardless of the heeling constraint, both F_{xs} and $|M_{xs}|$ will rise from 0 to their maximums while increasing $|\alpha_s|$ from 0 linearly. However, the maximums of them are inconsistent in $|\alpha_s|$. Denote the $|\alpha_s|$ corresponding to the maximum of F_{xs} as α_{su} and the $|\alpha_s|$ corresponding to the maximum of $|M_{xs}|$ as α_{sp}. If $\alpha_{aw} > 0$ and $\bar{M}_{xs}$ is bigger than the maximum of M_{xs}, or $\alpha_{aw} < 0$ and $\underline{M}_{xs}$ is smaller than the minimum of M_{xs}, we denote a threshold of $|\alpha_s|$ as $\alpha_{sl} = \alpha_{sp}$. Otherwise, it is derived from Eq. (3) that α_{sl} satisfies

$$\begin{cases} -\dfrac{\bar{M}_{xs}}{z_s} = L_s(\alpha_{sl})\cos(\alpha_{aw}) + D_s(\alpha_{sl})\sin(\alpha_{aw}), \ \alpha_{aw} > 0 \\ -\dfrac{\underline{M}_{xs}}{z_s} = L_s(-\alpha_{sl})\cos(\alpha_{aw}) + D_s(-\alpha_{sl})\sin(\alpha_{aw}), \ \alpha_{aw} < 0 \end{cases} \tag{11}$$

Then, $\bar{F}_{xs}$ is set to be the value of F_{xs} corresponding to $\min\{\alpha_{su}, \alpha_{sp}, \alpha_{sl}\}$, and the selecting range of Ω_s can be determined as a connected set corresponding to $F_{xs} \in [0, \bar{F}_{xs}]$, seeing Fig. 2. Because the sailboat is symmetric, Fig. 2 only delineates the condition that wind comes from the port side. In the upwind case, we assume that $\bar{M}_{xs}$ is bigger than the maximum of M_{xs}. Because C_{Ls} and C_{Ds} are not formulaic, Ω_s cannot be described with an analytical form. Nevertheless, it can be obtained through the numerical calculation. This is verified in the section of the numerical experiment. Thus, the heeling constraint is transformed to the input saturation of F_{xs} through the above design.

3.2. Sail

According to Lemma 1, the nonlinearity of the surge motion in Eq. (2) can be expressed as the FLS of Eq. (12).

$$\boldsymbol{W}_u^{\mathrm{T}}\boldsymbol{\varphi}_u(\upsilon) + \varepsilon_u = \frac{F_{xs} + m_v vr + F_{xh}}{m_u} \tag{12}$$

Following the backstepping approach, F_{xs}^c is first designed as

$$F_{xs}^c = m_u(-k_u u_e - \hat{\boldsymbol{W}}_u^{\mathrm{T}}\boldsymbol{\varphi}_u + \dot{u}_d) \tag{13}$$

where $k_u > 0$ is a tuning parameter. Invoking Eq. (5), the control error through the input saturation is denoted as $\Delta_u = \hat{F}_{xs} - F_{xs}^c$. According to the above analysis, we denote the value of δ_s corresponding to $\hat{F}_{xs}$ as $\hat{\delta}_s$. Define t_j^u as the triggering instant with $j = 0, 1, \ldots, +\infty$, and t_0^u is selected as the initial time t_0 of the voyage. Following the ETC, we set $\delta_s(t) = \hat{\delta}_s(t_j^u)$ in $t \in (t_j^u, t_{j+1}^u]$ and denote the control error as $e_u = F_{xs} - \hat{F}_{xs}$. Then, it yields $F_{xs} = F_{xs}^c + \Delta_u + e_u$. By differentiating u_e along Eqs. (2), (12) and (13), it renders

$$\dot{u}_e = \frac{e_u}{m_u} + \frac{\Delta_u}{m_u} - k_u u_e + \tilde{\boldsymbol{W}}_u^{\mathrm{T}}\boldsymbol{\varphi}_u + s_u \tag{14}$$

where $s_u = \varepsilon_u + d_{wu}$ and $\bar{s}_u = \bar{\varepsilon}_u + \bar{d}_{wu}$.

To offset the control error of Δ_u in Eq. (14), we design the auxiliary system as

$$\dot{\xi}_u = -\frac{\Delta_u}{m_u} - k_u\xi_u \tag{15}$$

where ξ_u is the auxiliary signal and $\beta_u = \xi_u + u_e$ implies the compensated tracking error. By synthesizing Eqs. (14) and (15), it yields

$$\dot{\beta}_u = \frac{e_u}{m_u} - k_u\beta_u + \tilde{\boldsymbol{W}}_u^{\mathrm{T}}\boldsymbol{\varphi}_u + s_u \tag{16}$$

Then, the next triggering instant t_{j+1}^u of δ_s is determined by the following triggering condition.

$$\begin{aligned} t_{j+1}^u &= \inf\{t \in \mathbb{R} | t > t_j^u \wedge e_u^2 \geq m_u^2(k_u - \frac{1}{2})(1-\gamma_u)\beta_u^2 \wedge \beta_u^2 > \eta_u\} \\ &\text{or} \\ t_{j+1}^u &= \inf\{t \in \mathbb{R} | t > t_j^u \wedge \delta_s(t) \notin \Omega_s\} \end{aligned} \tag{17}$$

where $0 < \gamma_u < 1$ and $\eta_u > 0$ are tuning parameters.

Remark 1. Similar with Deng et al. (2019e), the triggering condition of Eq. (17) cannot guarantee the existence of the minimum inter-event time due to the time-varying Ω_s. This is reflected in the second equation of Eq. (17). Nevertheless, the ETC design herein is to reduce the acting frequency of the sail. Compared with the continuous scheme, the saving of acting frequency is still remarkable.

3.3. Rudder

Following the backstepping approach, the virtual control law for r is designed as

$$\alpha_r = \frac{1}{\cos(\phi)}(-k_\psi\psi_e + \dot{\psi}_d) \tag{18}$$

where $k_\psi > 0$ is a tuning parameter. Denote the tracking error as $r_e = r - \alpha_r$. Differentiating ψ_e along Eqs. (18) and (1), it renders

$$\dot{\psi}_e = -k_\psi\psi_e + r_e\cos(\phi) \tag{19}$$

Design the auxiliary system as

$$\dot{\xi}_\psi = -k_\psi\xi_\psi + \xi_r\cos(\phi) \tag{20}$$

where ξ_ψ and ξ_r are auxiliary signals, $\beta_\psi = \xi_\psi + \psi_e$ and $\beta_r = \xi_r + r_e$ are compensated tracking errors. By synthesizing Eqs. (19) and (20), it renders

$$\dot{\beta}_\psi = -k_\psi\beta_\psi + \beta_r\cos(\phi) \tag{21}$$

According to Lemma 1, the nonlinearity of the yaw motion in Eq. (2) can be expressed as the following FLS.

$$\boldsymbol{W}_r^{\mathrm{T}}\boldsymbol{\varphi}_r(\upsilon) + \varepsilon_r = \frac{M_{zs} + (m_u - m_v)uv - d|r|r\cos(\phi) + M_{zh}}{m_r} \tag{22}$$

Then, δ_{r2}^c is designed as

$$\delta_{r2}^c = m_r\hat{\theta}\boldsymbol{\Phi}_r \tag{23}$$

and let $\boldsymbol{\Phi}_r = -k_r r_e - \hat{\boldsymbol{W}}_r^{\mathrm{T}}\boldsymbol{\varphi}_r - \beta_\psi\cos(\phi) + \dot{\alpha}_r$, where $k_r > 0$ is a tuning parameter and $\theta = 1/c_r$. From Eq. (18), it renders $\dot{\alpha}_r = (\cos(\phi)(k_\psi\dot{\psi}_d - k_\psi r + \ddot{\psi}_d) - \sin(\phi)p(k_\psi\psi_e - \dot{\psi}_d))/\cos^2(\phi)$. Thus, there is no difficulty in differentiating the virtual control law. Similarly, the control error through the input saturation is denoted as $\Delta_r = \hat{\delta}_{r2} - \delta_{r2}^c$. The triggering instant is denoted as t_j^r and t_0^r is assigned as t_0. We set $\delta_{r2}(t) = \hat{\delta}_{r2}(t_j^r)$

in $t \in (t_j^r, t_{j+1}^r]$ and let $e_r = \delta_{r2} - \hat{\delta}_{r2}$. Then, it has $\delta_{r2} = e_r + \Delta_r + \delta_{r2}^c$. By differentiating r_e along Eqs. (2), (22) and (23), it yields

$$\dot{r}_e = \frac{c_r \Delta_r}{m_r} + \frac{c_r e_r}{m_r} - k_r r_e + \tilde{\boldsymbol{W}}_r^{\mathrm{T}} \boldsymbol{\varphi}_r - \beta_\psi \cos(\phi) - c_r \tilde{\theta} \boldsymbol{\Phi}_r + s_r \tag{24}$$

where $s_r = \varepsilon_r + d_{wr}$ and $\bar{s}_r = \bar{\varepsilon}_r + \bar{d}_{wr}$. To offset the control error of Δ_r in Eq. (24), design the auxiliary system as

$$\dot{\xi}_r = -k_r \xi_r - \frac{\hat{c}_r \Delta_r}{m_r} \tag{25}$$

Synthesizing Eqs. (24) and (25), it renders

$$\dot{\beta}_r = \frac{\tilde{c}_r \Delta_r}{m_r} + \frac{c_r e_r}{m_r} - k_r \beta_r + \tilde{\boldsymbol{W}}_r^{\mathrm{T}} \boldsymbol{\varphi}_r - \beta_\psi \cos(\phi) - c_r \tilde{\theta} \boldsymbol{\Phi}_r + s_r \tag{26}$$

Then, the next triggering instant t_{j+1}^r of δ_{r2} is determined by the following triggering condition.

$$t_{j+1}^r = \inf\{t \in \mathbb{R} | t > t_j^r \wedge \hat{c}_r^2 e_r^2 \geq m_r^2 (k_r - \frac{1}{2})(1 - \gamma_r)\beta_r^2 \wedge \beta_r^2 > \eta_r\} \tag{27}$$

where $0 < \gamma_r < 1$ and $\eta_r > 0$ are tuning parameters.

3.4. Serial–parallel estimation model and adaptive laws

Because only the surge, roll and yaw motions in Eq. (2) are concerned, the serial–parallel estimation model is established only for these motions and as

$$\begin{cases} \dot{\hat{u}} = \dfrac{F_{xs}}{m_u} + \hat{\boldsymbol{W}}_u^{\mathrm{T}} \boldsymbol{\varphi}_u(\upsilon) + k_{fu} \tilde{u} \\ \dot{\hat{p}} = \dfrac{M_{xs}}{m_p} + \hat{\boldsymbol{W}}_p^{\mathrm{T}} \boldsymbol{\varphi}_p(\upsilon) + k_{fp} \tilde{p} \\ \dot{\hat{r}} = \dfrac{\hat{c}_r \delta_{r2}}{m_r} + \hat{\boldsymbol{W}}_r^{\mathrm{T}} \boldsymbol{\varphi}_r(\upsilon) + k_{fr} \tilde{r} \end{cases} \tag{28}$$

where $k_{fi} > 0$ with $i = u, p, r$ is the tuning parameter. By subtracting Eq. (28) from Eq. (2), we can obtain the differential equations of the prediction errors as

$$\begin{cases} \dot{\tilde{u}} = \tilde{\boldsymbol{W}}_u^{\mathrm{T}} \boldsymbol{\varphi}_u(\upsilon) - k_{fu} \tilde{u} + s_u \\ \dot{\tilde{p}} = \tilde{\boldsymbol{W}}_p^{\mathrm{T}} \boldsymbol{\varphi}_p(\upsilon) - k_{fp} \tilde{p} + s_p \\ \dot{\tilde{r}} = \dfrac{\tilde{c}_r \delta_{r2}}{m_r} + \tilde{\boldsymbol{W}}_r^{\mathrm{T}} \boldsymbol{\varphi}_r(\upsilon) - k_{fr} \tilde{r} + s_r \end{cases} \tag{29}$$

where $s_p = \varepsilon_p + d_{wp}$ and $\bar{s}_p = \bar{\varepsilon}_p + \bar{d}_{wp}$.

To be orchestrated with Eqs. (16), (26) and (29), the adaptive laws of $\boldsymbol{W}_u$, $\boldsymbol{W}_p$ and $\boldsymbol{W}_r$ are devised as

$$\begin{cases} \dot{\hat{\boldsymbol{W}}}_u = \boldsymbol{\Gamma}_u(\boldsymbol{\varphi}_u(\tilde{u} + \beta_u) - \sigma_u \hat{\boldsymbol{W}}_u) \\ \dot{\hat{\boldsymbol{W}}}_p = \boldsymbol{\Gamma}_p(\boldsymbol{\varphi}_p \tilde{p} - \sigma_p \hat{\boldsymbol{W}}_p) \\ \dot{\hat{\boldsymbol{W}}}_r = \boldsymbol{\Gamma}_r(\boldsymbol{\varphi}_r(\tilde{r} + \beta_r) - \sigma_r \hat{\boldsymbol{W}}_r) \end{cases} \tag{30}$$

where $\boldsymbol{\Gamma}_i$ is a positive definite matrix and $\sigma_i > 0$ is the tuning parameter with $i = u, p, r$.

To ensure the closed-loop stability in the following step, the uncertain gain of the rudder is estimated by the adaptive laws, and we devise

$$\begin{cases} \dot{\hat{\theta}} = \gamma_\theta(-\boldsymbol{\Phi}_r \beta_r - \sigma_\theta \hat{\theta}) \\ \dot{\hat{c}}_r = \gamma_c(\dfrac{e_r \beta_r}{m_r} + \dfrac{\Delta_r \beta_r}{m_r} + \dfrac{\tilde{r} \delta_{r2}}{m_r} - \sigma_c \hat{c}_r) \end{cases} \tag{31}$$

where γ_θ, γ_c, σ_θ and σ_c are positive tuning parameters.

Remark 2. It can be observed from Eq. (30) that the prediction errors of $\tilde{u}$, $\tilde{p}$ and $\tilde{r}$ are involved in the adaptive laws of the FLS weights, and combined with the compensated tracking errors of β_u and β_r. It can be observed from Eq. (29) that the prediction errors directly relate to the approximating accuracy of the FLSs. Thus, the terms of prediction errors in Eq. (30) function as the gradient descent algorithm for minimizing the prediction errors, and the proposed composite adaptive laws can reconcile the tracking performance with the approximating accuracy (Xu et al., 2014; Li and Tong, 2015; Li et al., 2016). Compared with the classic adaptive laws in Deng et al. (2019d), which belongs to the direct adaptive control (DAC) in Ioannou and Sun (1996), it leads to the smaller $\|\tilde{\boldsymbol{W}}_i\|$ with $i = u, p, r$. Nevertheless, σ_i should be bigger enough to prevent the parameter drifting.

4. Stability analysis

The result of this paper can be concluded as the following theorem.

Theorem 1. *Assume υ is defined in a compact set, namely the approximating capability of the FLSs is always guaranteed. For the sailboat described by Eqs. (1) and (2) and under the input saturation of Eqs. (5) and (6), if we adopt the control laws of Eqs. (13) and (23), the adaptive laws of Eqs. (30) and (31), and the triggering condition of Eqs. (17) and (27), all the tracking, the prediction and the estimating errors are ensured to be SGUUB. Besides, the heeling angle of ϕ is constrained in the interval of $(-\bar{\phi} - \mu/(k_p k_{\dot{p}}), \bar{\phi} + \mu/(k_p k_{\dot{p}}))$, where μ is a positive variable concerning the disturbance of d_{wp} and the estimating error of $\|\tilde{\boldsymbol{W}}_p\|$.*

Proof of SGUUB. Choose the Lyapunov function as $V = (\beta_\psi^2 + \beta_u^2 + \beta_r^2 + \tilde{u}^2 + \tilde{p}^2 + \tilde{r}^2 + \tilde{\boldsymbol{W}}_u^{\mathrm{T}} \boldsymbol{\Gamma}_u^{-1} \tilde{\boldsymbol{W}}_u + \tilde{\boldsymbol{W}}_p^{\mathrm{T}} \boldsymbol{\Gamma}_p^{-1} \tilde{\boldsymbol{W}}_p + \tilde{\boldsymbol{W}}_r^{\mathrm{T}} \boldsymbol{\Gamma}_r^{-1} \tilde{\boldsymbol{W}}_r)/2 + c_r \tilde{\theta}^2/(2\gamma_\theta) + \tilde{c}_r^2/(2\gamma_c)$. Consider $\beta_u^2 > \eta_u$ and $\beta_r^2 > \eta_r$, by differentiating V along Eqs. (16), (17), (21), (26), (27), (29), (30) and (31), it yields

$$\begin{aligned} \dot{V} =& \dot{\beta}_\psi \beta_\psi + \dot{\beta}_u \beta_u + \dot{\beta}_r \beta_r + \dot{u} \tilde{u} + \dot{\tilde{p}} \tilde{p} + \dot{\tilde{r}} \tilde{r} + \tilde{\boldsymbol{W}}_u^{\mathrm{T}} \boldsymbol{\Gamma}_u^{-1} \dot{\tilde{\boldsymbol{W}}}_u \\ &+ \tilde{\boldsymbol{W}}_p^{\mathrm{T}} \boldsymbol{\Gamma}_p^{-1} \dot{\tilde{\boldsymbol{W}}}_p + \tilde{\boldsymbol{W}}_r^{\mathrm{T}} \boldsymbol{\Gamma}_r^{-1} \dot{\tilde{\boldsymbol{W}}}_r + \frac{c_r}{\gamma_\theta} \dot{\tilde{\theta}} \tilde{\theta} + \frac{1}{\gamma_c} \dot{\tilde{c}}_r \tilde{c}_r \\ \leq& - k_\psi \beta_\psi^2 - \gamma_u (k_u - \frac{1}{2}) \beta_u^2 - \gamma_r (k_r - \frac{1}{2}) \beta_r^2 - \frac{c_r \sigma_\theta}{2} \tilde{\theta}^2 \\ &- (k_{fu} - \frac{1}{4}) \tilde{u}^2 - (k_{fp} - \frac{1}{4}) \tilde{p}^2 - (k_{fr} - \frac{1}{4}) \tilde{r}^2 - \frac{\sigma_c}{2} \tilde{c}_r^2 \\ &- \frac{\sigma_u}{2} \tilde{\boldsymbol{W}}_u^{\mathrm{T}} \tilde{\boldsymbol{W}}_u - \frac{\sigma_p}{2} \tilde{\boldsymbol{W}}_p^{\mathrm{T}} \tilde{\boldsymbol{W}}_p - \frac{\sigma_r}{2} \tilde{\boldsymbol{W}}_r^{\mathrm{T}} \tilde{\boldsymbol{W}}_r + \frac{\sigma_u}{2} \boldsymbol{W}_u^{\mathrm{T}} \boldsymbol{W}_u \\ &+ \frac{\sigma_p}{2} \boldsymbol{W}_p^{\mathrm{T}} \boldsymbol{W}_p + \frac{\sigma_r}{2} \boldsymbol{W}_r^{\mathrm{T}} \boldsymbol{W}_r + \frac{c_r \sigma_\theta}{2} \theta^2 + \frac{\sigma_c}{2} c_r^2 + \bar{s}_p^2 \\ &+ 2\bar{s}_r^2 + 2\bar{s}_u^2 \end{aligned} \tag{32}$$

Select $k_\psi, k_u > 1/2$, $k_r > 1$ and $k_{fu}, k_{fp}, k_{fr} > 1/4$. Define $\zeta = \min\{2k_{fu} - 1/2, 2k_{fp} - 1/2, 2k_{fr} - 1/2, 2\gamma_u k_u - \gamma_u, 2\gamma_r k_r - \gamma_r, 2k_\psi, \sigma_\theta \gamma_\theta, \sigma_c \gamma_c, \sigma_u \lambda_{min}(\boldsymbol{\Gamma}_u), \sigma_p \lambda_{min}(\boldsymbol{\Gamma}_p), \sigma_r \lambda_{min}(\boldsymbol{\Gamma}_r)\}$, where $\lambda_{min}(\cdot)$ denotes the minimum eigenvalue of the matrix. Let $\varrho = \sigma_u \boldsymbol{W}_u^{\mathrm{T}} \boldsymbol{W}_u/2 + \sigma_p \boldsymbol{W}_p^{\mathrm{T}} \boldsymbol{W}_p/2 + \sigma_r \boldsymbol{W}_r^{\mathrm{T}} \boldsymbol{W}_r/2 + c_r \sigma_\theta \theta^2/2 + \sigma_c c_r^2/2 + \bar{s}_p^2 + 2\bar{s}_r^2 + 2\bar{s}_u^2$. Then, Eq. (32) is transformed to

$$\dot{V} \leq -\zeta V + \varrho \tag{33}$$

Through the comparison theorem, it can be inferred from Eq. (33) that $V(t) \leq (V(t_0) - \varrho/\zeta) \exp(-\zeta(t - t_0)) + \varrho/\zeta$ holds. Thus, all the errors in V are SGUUB and β_i^2 is ultimately bounded by $\max\{\eta_i, 2\varrho/\zeta\}$ with $i = u, r$.

Further, the SGUUB of the tracking errors, namely ψ_e, u_e and r_e, can be proven. Choose the Lyapunov candidate as $V_\xi = (\xi_\psi^2 + \xi_u^2 + \xi_r^2)/2$. Differentiating V_ξ along Eqs. (15), (20) and (25), it renders

$$\begin{aligned} \dot{V}_\xi =& \dot{\xi}_\psi \xi_\psi + \dot{\xi}_u \xi_u + \dot{\xi}_r \xi_r \\ \leq& - (k_\psi - \frac{1}{2}) \xi_\psi^2 - (k_u - \frac{1}{2}) \xi_u^2 - (k_r - 1) \xi_r^2 + \frac{\Delta_u^2}{2m_u^2} \\ &+ \frac{\hat{c}_r^2 \Delta_r^2}{2m_r^2} \end{aligned} \tag{34}$$

Define $\zeta_\xi = \min\{2k_\psi - 1, 2k_u - 1, 2k_r - 2\}$ and $\varrho_\xi = \Delta_u^2/(2m_u^2) + \hat{c}_r^2 \Delta_r^2/(2m_r^2)$. Then, Eq. (34) can be transformed to

$$\dot{V}_\xi \leq -\zeta_\xi V_\xi + \varrho_\xi \tag{35}$$

Through the comparison theorem, it can be inferred from Eq. (35) that $V_\xi(t) \leq (V_\xi(t_0) - \varrho_\xi/\zeta_\xi) \exp(-\zeta_\xi(t - t_0)) + \varrho_\xi/\zeta_\xi$. According to the

composition of ϱ_ξ, we can conclude that V_ξ is asymptotically stable if $\Delta_u = \Delta_r = 0$ and is SGUUB if Δ_u and Δ_r keep bounded. Choose the Lyapunov candidate of the tracking errors as $V_t = (\psi_e^2 + u_e^2 + r_e^2)/2$. By using the inequalities of $\psi_e^2 \le 2\beta_\psi^2 + 2\xi_\psi^2$, $u_e^2 \le 2\beta_u^2 + 2\xi_u^2$ and $r_e^2 \le 2\beta_r^2 + 2\xi_r^2$, it further yields $V_t \le 2V + 2V_\xi$. According to the above analysis of V and V_ξ, it is clear that ψ_e, u_e and r_e in V_t are SGUUB.

Remark 3. Because υ is defined in a compact set, the control laws in Eqs. (13) and (23) are bounded. From the definitions of Δ_u and Δ_r, it is reasonable to assume that Δ_u and Δ_r keep bounded in the above analysis. While the input saturation does not work, namely $\Delta_u = \Delta_r = 0$, we have $\psi_e \to \beta_\psi$, $u_e \to \beta_u$ and $r_e \to \beta_r$. Because the input saturation will limit the control energies, it is not practical to stabilize ψ_e, u_e and r_e directly. For example, the closed-loop stability is degraded in the existing literature of Ma et al. (2019), Deng et al. (2019a) and Zheng et al. (2018). The auxiliary systems in this paper can successfully circumvent this problem. They were widely used to deal with the input saturation in Li and Tong (2015) and Du et al. (2016) and eliminate the analytical differentiation of the virtual control laws in Dong et al. (2012) and Zhu et al. (2018).

Remark 4. It can be inferred from Eq. (33) that by choosing k_{fu}, k_{fp}, k_{fr}, k_u, k_r, k_ψ, γ_u, γ_r, γ_θ, γ_c, $\lambda_{min}(\mathbf{\Gamma}_u)$, $\lambda_{min}(\mathbf{\Gamma}_p)$ and $\lambda_{min}(\mathbf{\Gamma}_r)$ largely enough, the compensated tracking errors and the prediction errors can be regulated into any small bound with a fast convergent rate. Nevertheless, this setting may lead to an undesired transient and the waste of control energy. As is mentioned in Remark 3, the saturation constraint will also affect the convergence of the tracking errors. Besides, it can be inferred from Eqs. (17) and (27) that the growth of γ_u and γ_r will increase the acting frequencies of the actuators. Thus, the selection of these parameters should be devoted to the desired closed-loop response and practical needs.

Remark 5. One can follow Jiao and Wang (2016a,b) and Deng et al. (2019a,e) to prove the existence of the minimum inter-event time of the sail in the first equation of Eq. (17) and that of the rudder in Eq. (27). In brief, the control errors of e_u and e_r are reset to 0 at the triggering instants, and the growth rates of e_u^2 and $\hat{c}_r e_r^2$ are bounded in the compact set, while the triggering thresholds are ensured to be bigger than $m_u^2(k_u - 1/2)(1-\gamma_u)\eta_u$ and $m_r^2(k_r - 1/2)(1-\gamma_r)\eta_r$, a minimum time is always ensured for e_u^2 and $\hat{c}_r e_r^2$ to rise from 0 to the triggering thresholds.

Remark 6. According to Krstić et al. (1995), the smoothness of control inputs is one of sufficient conditions to ensure the feasibility of the backstepping method, whereas the control inputs of δ_s and δ_{r2} are unsmooth at the triggering instant in this paper. Nevertheless, the unsmooth control inputs herein will not damage the application of backstepping. For this purpose, we can refer to the tool of "impulsive dynamical system" in Haddad et al. (2006). While it denotes the jumps of V and V_t at the triggering instant as ΔV and ΔV_t, it is clear from Eq. (2) that $\Delta V = \Delta V_t = 0$. Because δ_s and δ_{r2} keep unchanged and smooth during the inter-event time, the convergence of V and V_t is guaranteed in the entire time domain, which illustrates the feasibility of backstepping in this paper. For the case of $\Delta V \neq 0$, a more complex analysis is required, seeing Deng et al. (2019b).

Proof of heeling constraint. While F_{xs} is bounded by the derived $\bar{F}_{xs}$, it holds $\underline{M}_{xs} \le M_{xs} \le \bar{M}_{xs}$ during the voyage. By substituting Eqs. (10) to (2), it yields

$$\begin{cases} \dot{p} \ge k_{\dot{p}}(\underline{p} - p) + \dot{\underline{p}} - |\tilde{\boldsymbol{W}}_p^{\mathrm{T}} \boldsymbol{\varphi}_p| - \bar{d}_{wp} \\ \dot{p} \le k_{\dot{p}}(\bar{p} - p) + \dot{\bar{p}} + |\tilde{\boldsymbol{W}}_p^{\mathrm{T}} \boldsymbol{\varphi}_p| + \bar{d}_{wp} \end{cases} \tag{36}$$

Define $\mu = \|\tilde{\boldsymbol{W}}_p\|^2/2 + 1/2 + \bar{d}_{wp}$. By solving Eq. (36) through the comparison theorem, one can obtain

$$\begin{cases} p(t) \ge \underline{p}(t) - \dfrac{\mu}{k_{\dot{p}}} + (p(t_0) - \underline{p}(t_0) + \dfrac{\mu}{k_{\dot{p}}}) \exp(-k_{\dot{p}}(t - t_0)) \\ p(t) \le \bar{p}(t) + \dfrac{\mu}{k_{\dot{p}}} + (p(t_0) - \bar{p}(t_0) - \dfrac{\mu}{k_{\dot{p}}}) \exp(-k_{\dot{p}}(t - t_0)) \end{cases} \tag{37}$$

It can be inferred from Eq. (37) that if $\underline{p}(t_0) < p(t_0) < \bar{p}(t_0)$ holds, $\underline{p}(t) - \mu/k_{\dot{p}} < p(t) < \bar{p}(t) + \mu/k_{\dot{p}}$ always holds. By substituting Eqs. (8) to (1), it yields

$$\begin{cases} \dot{\phi} > -k_p(\bar{\phi} + \phi) - \dfrac{\mu}{k_{\dot{p}}} \\ \dot{\phi} < k_p(\bar{\phi} - \phi) + \dfrac{\mu}{k_{\dot{p}}} \end{cases} \tag{38}$$

By solving Eq. (38) through the comparison theorem, one can obtain

$$\begin{cases} \phi(t) > -\bar{\phi} - \dfrac{\mu}{k_p k_{\dot{p}}} + (\phi(t_0) + \bar{\phi} + \dfrac{\mu}{k_p k_{\dot{p}}}) \exp(-k_p(t - t_0)) \\ \phi(t) < \bar{\phi} + \dfrac{\mu}{k_p k_{\dot{p}}} + (\phi(t_0) - \bar{\phi} - \dfrac{\mu}{k_p k_{\dot{p}}}) \exp(-k_p(t - t_0)) \end{cases} \tag{39}$$

It can be inferred from Eq. (39) that if $-\bar{\phi} < \phi(t_0) < \bar{\phi}$ initially holds, $-\bar{\phi} - \mu/(k_p k_{\dot{p}}) < \phi(t) < \bar{\phi} + \mu/(k_p k_{\dot{p}})$ always holds. Because $\|\tilde{\boldsymbol{W}}_p\|$ in μ is bounded according to the above analysis, it is known that the varying range of $(-\bar{\phi} - \mu/(k_p k_{\dot{p}}), \bar{\phi} + \mu/(k_p k_{\dot{p}}))$ will converge to $[-\bar{\phi}, \bar{\phi}]$ by increasing k_p and $k_{\dot{p}}$. The proof is completed.

5. Numerical experiment

A 12 m sailing yacht is chosen to be the experimental objective. It was also adopted in Xiao and Jouffroy (2014) and Deng et al. (2019d). The author can refer to these literature for the detailed parameters. The lift and drag coefficients of the sail are provided in Fig. 3 corresponding to the attacking angle of α_s. Here, the path-following task is carried out to verify the effectiveness of the proposed scheme. The curved reference path is described by the sinusoidal function of $x_d = 150\sin(\pi y_d/100) + 50$ with $y_d \in [0\text{ m}, 500\text{ m}]$, where x_d and y_d are the positional coordinates of the reference path. The parallel guidance principle in Deng et al. (2019e) is adopted to generate the desired heading angle of ψ_d, and the desired surge speed of u_d is selected as 2 m/s. The true wind is set with the speed of 6 m/s, which points to the south and revolves anti-clockwise with the constant rate of 0.01°/s. The simplified disturbances are described by the first-order Markov process as Eq. (40).

$$\begin{cases} \dot{d}_{wu} = -0.1 d_{wu} + 0.05\omega_u \\ \dot{d}_{wv} = -0.1 d_{wv} + 0.05\omega_v \\ \dot{d}_{wp} = -0.1 d_{wp} + 0.02\omega_p \\ \dot{d}_{wr} = -0.1 d_{wr} + 0.02\omega_r \end{cases} \tag{40}$$

where ω_i with $i = u, v, p, \upsilon$ is the Gauss white noise with the variance of 1. The initial positional coordinates, attitudes and kinematic states of the sailboat are set as $x(t_0) = y(t_0) = 0$ m, $\psi(t_0) = 45°$, $\phi(t_0) = 0°$, $u(t_0) = v(t_0) = 0$ m/s and $p(t_0) = r(t_0) = 0°/\text{s}$.

To outstand the advantages of the proposed scheme, the event-triggered robust fuzzy damping control scheme in Deng et al. (2019e) is selected for comparison. The heeling constraint is not considered in that scheme, and the parameters are regulated to preserve the best control performances. The sailboat with that scheme is marked as No.1. To demonstrate the advantages of the composite learning, we set another comparison of the customary direct adaptive control. Different with Eq. (30), the adaptive laws of FLS weights in this scheme are devised as

$$\begin{cases} \dot{\hat{\boldsymbol{W}}}_u = \mathbf{\Gamma}_u(\boldsymbol{\varphi}_u \beta_u - \sigma_u \hat{\boldsymbol{W}}_u) \\ \dot{\hat{\boldsymbol{W}}}_p = \mathbf{\Gamma}_p(\boldsymbol{\varphi}_p p - \sigma_p \hat{\boldsymbol{W}}_p) \\ \dot{\hat{\boldsymbol{W}}}_r = \mathbf{\Gamma}_r(\boldsymbol{\varphi}_r \beta_r - \sigma_r \hat{\boldsymbol{W}}_r) \end{cases} \tag{41}$$

Table 2
Quantified control performances.

Indexes	No.1 sailboat	No.2 sailboat	No.3 sailboat
ψ_{em}	1.29°	2.03°	1.61°
u_{em}	1.03 m/s	1.10 m/s	1.07 m/s
ϕ_{max}	48.66°	30.40°	29.60°
N_s	10 254	7050	6568
N_r	14 278	12 775	13 766
t_{end}	1767.3 s	1979.5 s	1800.9 s
Memory	7376 kb	10 244 kb	11 772 kb

where the prediction errors are exempted and the serial–parallel estimation model of Eq. (28) is not required. The sailboat with this scheme is marked as No.2. Finally, the sailboat with the proposed composite adaptive scheme in this paper is marked as No.3. It should be noted that all the parameters of the No.2 and the No.3 sailboats keep the same and are presented as Eq. (42).

$$\begin{aligned} &k_\psi = 0.5,\ k_u = 0.1,\ k_r = 0.2,\ k_p = k_{\dot{p}} = 1,\ \gamma_u = 0.6,\\ &\gamma_r = 0.8,\ k_{fu} = k_{fp} = k_{fr} = 0.1,\ \eta_u = \eta_r = 0.5,\\ &\boldsymbol{\Gamma}_u = \boldsymbol{\Gamma}_p = \boldsymbol{\Gamma}_r = 0.1\boldsymbol{I}_{5\times5},\ \sigma_u = \sigma_p = \sigma_r = 0.1,\\ &\gamma_\theta = \gamma_c = 0.1,\ \sigma_\theta = \sigma_c = 1. \end{aligned} \tag{42}$$

The threshold of the heeling angle is set as $\bar{\phi} = 30°$. Then, the numerical experiment is carried out in the environment of MATLAB. The results are shown in Figs. 4–13 and the quantified control performances are provided in Table 2.

Fig. 4 exhibits the trajectories of the three sailboats. The parallel guidance principle works well and all the three sailboats can track the reference path in a satisfactory accuracy. In this figure, the No.1 and the No.3 sailboats behave better than the No.2. Define the average tracking errors as Eq. (43).

$$\begin{cases} \psi_{em} = \displaystyle\int_{t_0}^{t_{end}} |\psi_e(\tau)|\mathrm{d}\tau \\ u_{em} = \displaystyle\int_{t_0}^{t_{end}} |u_e(\tau)|\mathrm{d}\tau \end{cases} \tag{43}$$

where t_{end} is the total voyage time. It can be found in Table 2 that ψ_{em}, u_{em} and t_{end} of the No.2 are bigger than those of the No.1 and the No.3. This suggests the tracking performance of the No.2 is degraded due to the inaccurate approximation of the FLSs. Fig. 5 shows the evolution of the disturbances within 1700 s. The first-order Markov process can embodies the features of the waves in a normal sea condition with fidelity. Fig. 6 exhibits the evolution of the kinematic states. According to the analysis in Remark 3, it is reasonable that u cannot always reach the desired value of u_d. The speed loss of u inevitably happens at the tacking maneuver. v is passively bounded and its overshoots occur at the tacking maneuver. p oscillates drastically but keeps bounded during the voyage. The overshoots of r occur while the sailboats turn. The above speed responses are reasonable for the sailboat. Fig. 7 exhibits the evolution of the heeling angles. It can be observed that ϕ of the No.2 and the No.3 sailboats are nearly bounded by the red dashed lines of $\pm\bar{\phi}$ during the voyage, whereas the No.1 often breaks through the threshold while the sailboat turns. The maximum heeling angles of ϕ_{max} are provided in Table 2. The ϕ_{max} of the No.2 is a little bigger than $\bar{\phi}$, which is caused by $\mu/(k_p k_{\dot{p}})$ according to the above proof. It should be noted that the proposed scheme sacrifices the thrust of the sail for satisfying the heeling constraint. Thus, the average of u in the No.2 and the No.3 sailboats is slower than that in the No.1, such that t_{end} of them is also longer than that of the No.1 in Table 2.

Fig. 8 demonstrates the control inputs of δ_s and δ_r. Affected by the disturbances, both of them oscillate drastically during the voyage. The saturation of δ_r occurs while the sailboat turns. It can be observed from the local enlarged view at 650–680 s of Fig. 8(b) that the control inputs hold during the inter-event time and the event-triggered mechanism works. Fig. 9 shows the accumulation of triggering times within

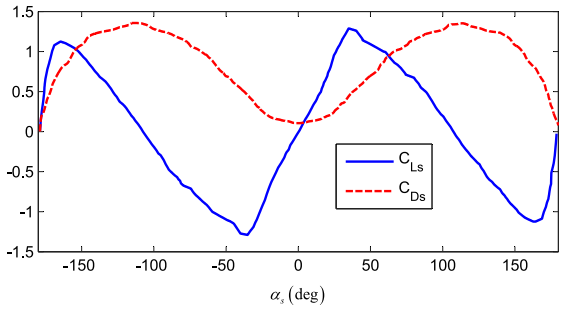

Fig. 3. Lift and drag coefficients.

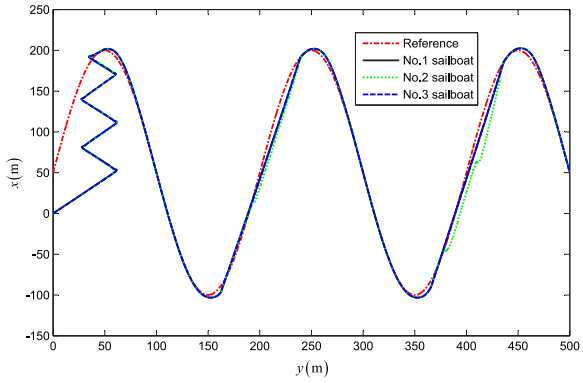

Fig. 4. Planar trajectories.

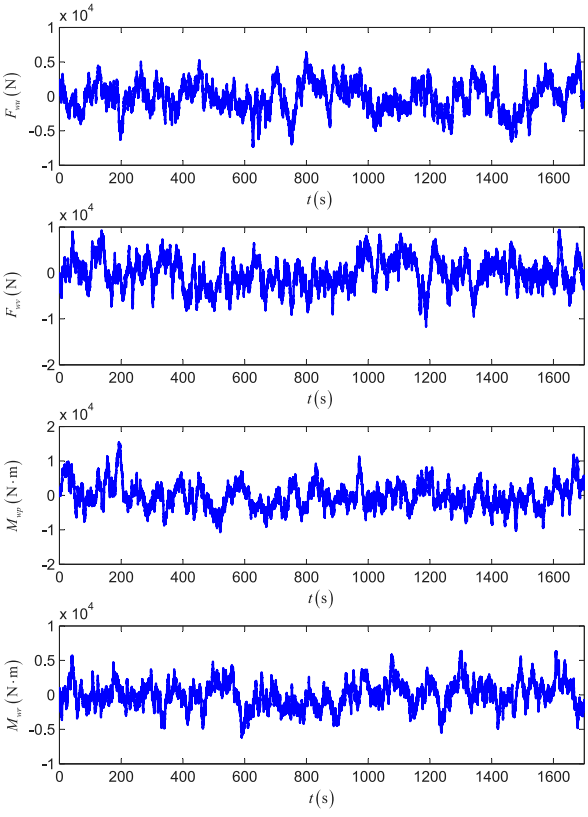

Fig. 5. Disturbances.

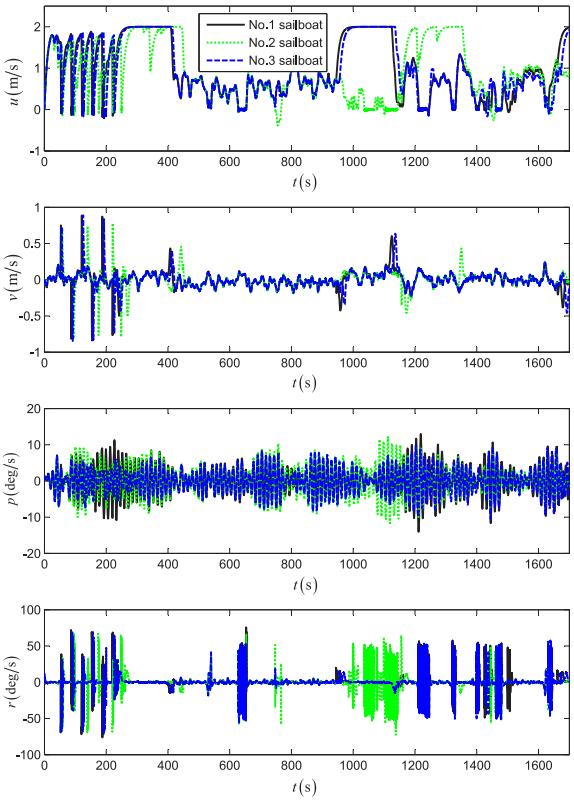

Fig. 6. Kinematic states.

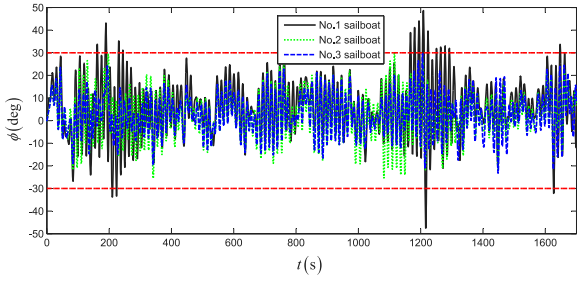

Fig. 7. Heeling angle.

1700 s. Compared with the continuous scheme, the saving of acting frequencies is remarkable in three sailboats. It can be observed that the accumulation in the No.1 grows faster than that in the others due to the conservatism of the robust control. The total accumulation at 1700 s of the sail and the rudder are denoted as N_s and N_r respectively, which are provided in Table 2. Fig. 10 provides the $|\alpha_s|$ of the No.3 sailboat corresponding to α_{sp}, α_{su} and α_{sl} respectively. During the voyage, the varying range of $|\alpha_s|$ is determined from 0 to the minimum of these three curves.

Fig. 11 compares the approximating errors of the FLSs in the No.2 and the No.3 sailboats. It can be observed that the approximating error of the No.3 is significantly smaller than that of the No.2. The composite learning of the FLSs is effective in identifying the uncertainties. Fig. 12 demonstrates the evolution of $\|\hat{\boldsymbol{W}}_u\|$, $\|\hat{\boldsymbol{W}}_p\|$ and $\|\hat{\boldsymbol{W}}_r\|$, while Fig. 13 demonstrates the evolution of $\hat{\theta}$ and $\hat{c}_r$ in the No.3 sailboat. According to the stability analysis, all of them tend to be bounded. It should be noted that the design in Eq. (31) belongs to DAC such that $\hat{\theta}\hat{c}_r = 1$ is not achievable in Fig. 13.

The computational simplicity of three control schemes is also compared in this simulation. Through the "profile" function in MATLAB,

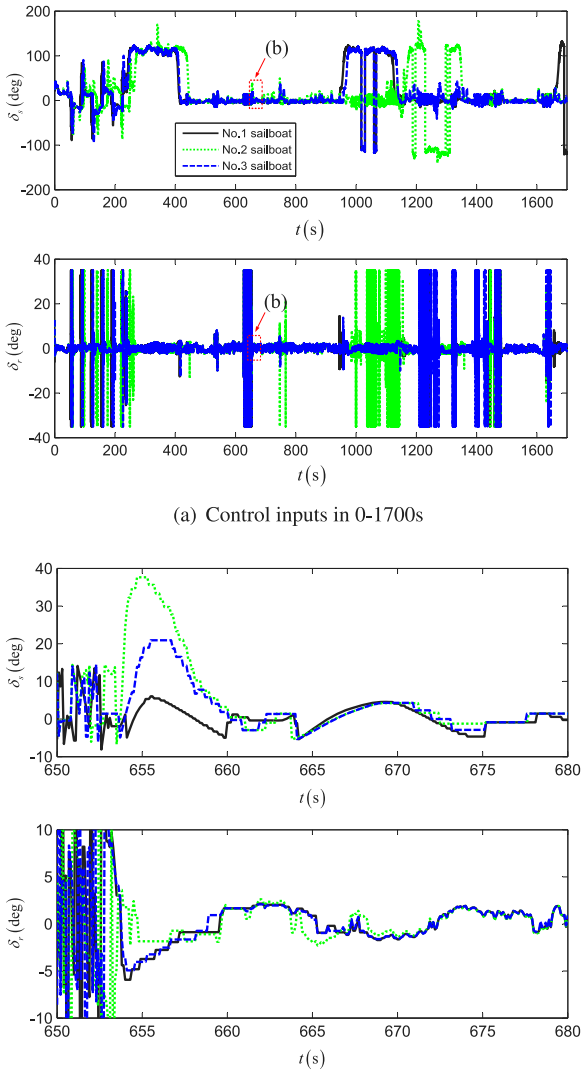

(a) Control inputs in 0-1700s

(b) Local enlarged diagram

Fig. 8. Control inputs.

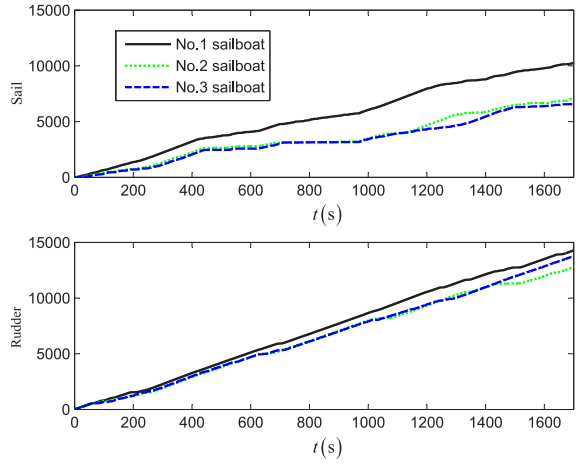

Fig. 9. Accumulation of triggering times.

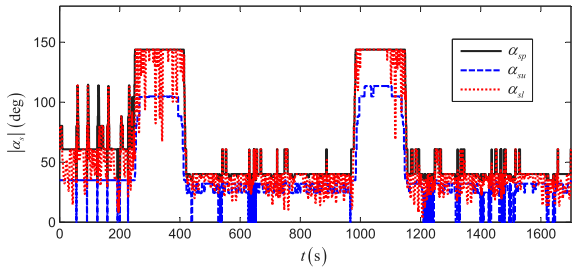

Fig. 10. Scopes of attacking angles.

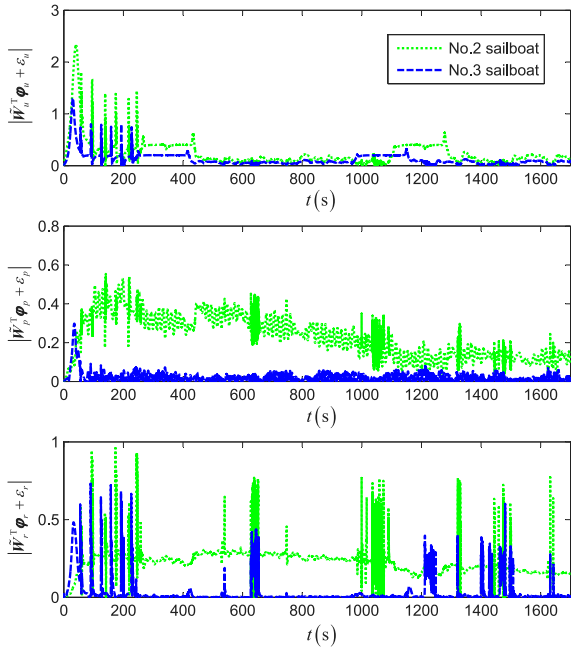

Fig. 11. Approximating errors.

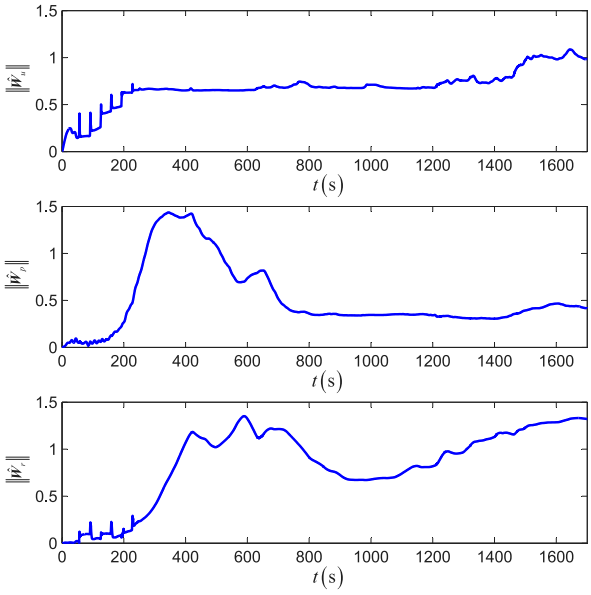

Fig. 12. Estimated FLS weights.

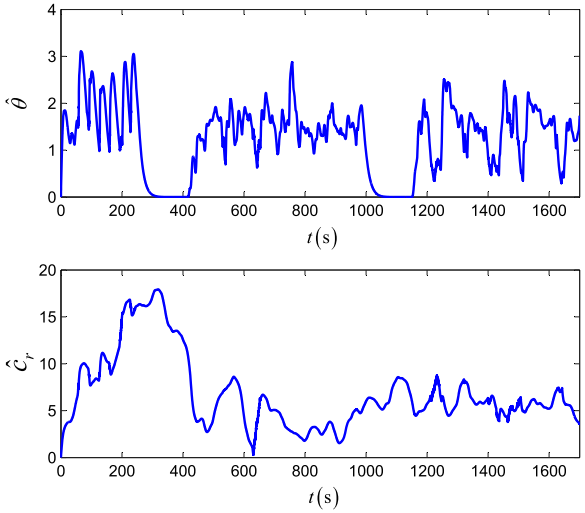

Fig. 13. Adaptive parameters.

we record the memory occupation of the three programs during their running time. From Table 2, it is found that the robust damping in Deng et al. (2019e) is the most succinct one. This is because the adaptive laws are not required in that scheme. However, the proposed control scheme can outperform the robust damping one in less conservatism.

6. Conclusion

This paper investigates the event-triggered composite adaptive fuzzy control of the sailboat in the surge speed and the heading angle. In addition, the heeling constraint is considered during the voyage. The serial–parallel estimation model is constructed to evaluate the approximating accuracy of the FLSs, and the prediction errors are involved in the composite adaptive laws. With the known aerodynamics of the sail, the heeling constraint is transformed to the input saturation of the sail. The auxiliary systems are fabricated to offset the input saturation. The ETC laws are separately built for the sail and the rudder with the triggering conditions. The uncertain gain of the rudder is estimated by the adaptive laws. Finally, the proposed control scheme is matched with the path-following guidance principle in Deng et al. (2019e), and the fine control performances are observed in the simulation. This paper is deemed as a phase summary of our work in the control of the sailboat. In the future, we can improve this scheme with output feedback and get enlightened from Li and Tong (2015) and Li et al. (2016).

CRediT authorship contribution statement

Yingjie Deng: Writing - orignial draft, Writing - review & editing. **Xianku Zhang:** Conceptualization, Supervision. **Qiang Zhang:** Software, Validation. **Yancai Hu:** Investigation, Writing - review & editing.

Declaration of competing interest

The authors declare that they have no known competing financial interests or personal relationships that could have appeared to influence the work reported in this paper.

Acknowledgments

This work is partially supported by National Science Foundation of China (No. 51679024), Fundamental Research Funds for the Central University, China (No. 3132019501), University 111 Project of China

(No. B08046), National Science Foundation of Shandong Jiaotong University, China (No. Z201631), Key Research and Development Plan of Shandong Province, China (No. 2019JZZY020712), and Shandong Jiaotong University Phd Startup Foundation of Scientific Research, China.

References

Cao, L., Li, H., Zhou, Q., 2018. Adaptive intelligent control for nonlinear strict-feedback systems with virtual control coefficients and uncertain disturbances based on event-triggered mechanism. IEEE Trans. Cybern. 48 (12), 3390–3402.

Corno, M., Formentin, S., Savaresi, S.M., 2016. Data-driven online speed optimization in autonomous sailboats. IEEE Trans. Intell. Transp. Syst. 17 (3), 762–771.

Cruz, N.A., Alves, J.C., 2010. Auto-heading controller for an autonomous sailboat. In: Oceans. IEEE, pp. 1–6.

Deng, Y., Zhang, X., Im, N., Zhang, G., Zhang, Q., 2019a. Event-triggered robust fuzzy path following control for underactuated ships with input saturation. Ocean Eng. http://dx.doi.org/10.1016/j.oceneng.2019.106122.

Deng, Y., Zhang, X., Im, N., Zhang, G., Zhang, Q., 2019b. Model-based event-triggered tracking control of underactuated surface vessels with minimum learning parameters. IEEE Trans. Neural Netw. Learn. Syst. http://dx.doi.org/10.1109/tnnls.2019.2951709.

Deng, Y., Zhang, X., Zhang, G., 2019c. Fuzzy logic based speed optimization and path following control for sail-assisted ships. Ocean Eng. 171, 300–310.

Deng, Y., Zhang, X., Zhang, G., 2019d. Line-of-sight-based guidance and adaptive neural path-following control for sailboats. IEEE J. Ocean. Eng. http://dx.doi.org/10.1109/JOE.2019.2923502.

Deng, Y., Zhang, X., Zhang, G., Huang, C., 2019e. Parallel guidance and event-triggered robust fuzzy control for path following of autonomous wing-sailed catamaran. Ocean Eng. http://dx.doi.org/10.1016/j.oceneng.2019.106442.

Do, K.D., 2010. Practical control of underactuated ships. Ocean Eng. 37, 1111–1119.

Dong, W., Farrell, J.A., Polycarpou, M.M., Djapic, V., Sharma, M., 2012. Command filtered adaptive backstepping. IEEE Trans. Control Syst. Technol. 20 (3), 566–580.

Du, J., Hu, X., Krstić, M., Sun, Y., 2016. Robust dynamic positioning of ships with disturbances under input saturation. Automatica 73, 207–214.

Elkaim, G., Kelbley, R., 2006. Station keeping and segmented trajectory control of a wind-propelled autonomous catamaran. In: IEEE Conference on Decision and Control. IEEE, pp. 2424–2429.

Guo, X., Yan, W., Cui, R., 2019. Event-triggered reinforcement learning-based adaptive tracking control for completely unknown continuous-time nonlinear systems. IEEE Trans. Cybern. http://dx.doi.org/10.1109/tcyb.2019.2903108.

Haddad, W.M., Chellaboina, V., Nersesov, S.G., 2006. Impulsive and Hybrid Dynamical Systems: Stability, Dissipativity, and Control. Princeton University Press, Princeton.

He, J., Xiao, L., Jouffroy, J., 2012. Towards heading control of an autonomous sailing platform through weight balancing. In: 9th IFAC Conference on Manoeuvring and Control of Marine Craft. IFAC, pp. 392–397.

Herrero, P., Jaulin, L., Vehí, J., Sainz, M.A., 2010. Guaranteed set-pointed computation with application to the control of a sailboat. Int. J. Control Autom. Syst. 8 (1), 1–7.

Ioannou, P., Sun, J., 1996. Robust Adaptive Control. Prentice Hall, Upper Saddle River.

Jaulin, L., Bars, F.L., 2013. An intervel approach for stability analysis: Application to sailboat robotics. IEEE Trans. Robot. 29 (1), 282–287.

Jiang, Z., 2002. Global tracking control of underactuated ships by lyapunov's direct method. Automatica 38, 301–309.

Jiao, J., Wang, G., 2016a. Event driven tracking control algorithm for marine vessel based on backstepping method. Neurocomputing 207, 669–675.

Jiao, J., Wang, G., 2016b. Event triggered trajectory tracking control approach for fully actuated surface vessel. Neurocomputing 182, 267–273.

Krstić, M., Kanellakopoulos, I., Kokotović, P., 1995. Nonlinear and Adaptive Control Design. John Wiley & Sons, New York.

Li, J., Lee, P., Jun, B., Lim, Y., 2008. Point-to-point navigation of underactuated ships. Automatica 44 (12), 3201–3205.

Li, Y., Tong, S., 2015. Composite adaptive fuzzy output feedback control design for uncertain nonlinear strict-feedback systems with input saturation. IEEE Trans. Cybern. 45, 2299–2308.

Li, Y., Tong, S., Li, T., 2016. Hybrid fuzzy adaptive output feedback control design for uncertain mimo nonlinear systems with time-varying delays and input saturation. IEEE Trans. Fuzzy Syst. 24, 841–853.

Li, Y., Yang, G., 2018. Adaptive neural control of pure-feedback nonlinear systems with event-triggered communications. IEEE Trans. Neural Netw. Learn. Syst. 29 (12), 6242–6251.

Ma, Y., Zhu, G., Liu, Z., 2019. Error-driven-based nonlinear feedback recursive design for adaptive nn trajectory tracking control of surface ships with input saturation. IEEE Intell. Transp. Syst. Mag. 11, 17–28.

Peng, Z., Wang, J., Wang, J., 2019. Constrained control of autonomous underwater vehicles based on command optimization and disturbance estimation. IEEE Trans. Ind. Electron. 66 (5), 3627–3635.

Saoud, H., Hua, M.D., Plumet, F., Amar, F.B., 2015. Routing and course control of an autonomous sailboat. In: European Conference on Mobile Robots. IEEE, pp. 1–6.

Shen, Z., Wang, S., Yu, H., Guo, C., 2019. Online speed optimization with feedforward of unmanned sailboat via extremum seeking without steady-state oscillation. Ocean Eng. http://dx.doi.org/10.1016/j.oceaneng.2019.106393.

Stelzer, R., Pröll, T., John, R.I., 2007. Fuzzy logic control system for autonomous sailboats. In: IEEE International Fuzzy Systems Conference. pp. 1–6.

Stevens, B.L., Lewis, F.L., Johnson, E.N., 2016. Aircraft Control and Simulation: Dynamics, Controls Design, and Autonomous Systems, third Ed.. John Wiley & Sons, Hoboken.

Wang, L., 1994. Adaptive Fuzzy Systems and Control: Design and Stability Analysis. Prentice Hall, New Jersey, US.

Xiao, L., Alves, J.C., Cruz, N.A., Jouffroy, J., 2012. Online speed optimization for sailing yachts using extremum seeking. In: Oceans. IEEE, pp. 1–6.

Xiao, L., Jouffroy, J., 2011. Modeling and nonlinear heading control for sailing yachts. In: Oceans. IEEE, pp. 1–6.

Xiao, L., Jouffroy, J., 2014. Modeling and nonlinear heading control of sailing yachts. IEEE J. Ocean. Eng. 39 (2), 256–268.

Xu, B., Shi, Z., Yang, C., Sun, F., 2014. Composite neural dynamic surface control of a class of uncertain nonlinear systems in strict-feedback form. IEEE Trans. Cybern. 44 (12), 2626–2634.

Yan, Z., Wang, J., 2012. Model predictive control for tracking of underactuated vesseks based on recurrent neural networks. IEEE Trans. Ocean. Eng. 37 (4), 717–726.

Zhang, G., Deng, Y., Zhang, W., Huang, C., 2018. Novel dvs guidance and path-following control for underactuated ships in presence of multiple static and moving obstacles. Ocean Eng. 170, 100–110.

Zheng, Z., Sun, L., Xie, L., 2018. Error-constrained los path following of a surface vessel with actuator saturation and faults. IEEE Trans. Syst. Man Cybern.: Syst. 48 (10), 1794–1805.

Zhu, G., Du, J., Kao, Y., 2018. Command filtered robust adaptive nn control for a class of uncertain strict-feedback nonlinear systems under input saturation. J. Franklin Inst. B 355 (15), 7548–7569.